Josephson-Anderson relation as diagnostic of turbulent drag reduction by polymers

Samvit Kumar,[1] Simon Toedtli,[2] Tamer A. Zaki,[1,2] and Gregory L. Eyink[1,2,3]
[1]*Department of Applied Mathematics & Statistics, Johns Hopkins University, Baltimore, Maryland 21218, USA*
[2]*Department of Mechanical Engineering, Johns Hopkins University, Baltimore, Maryland 21218, USA*
[3]*Department of Physics & Astronomy, The Johns Hopkins University, Baltimore, Maryland 21218, USA*

(Received 21 February 2024; accepted 12 December 2024; published 24 January 2025)

The detailed Josephson-Anderson relation, which equates instantaneously the volume-integrated vorticity flux and the work by pressure drop, has been the key to drag reduction in superconductors and superfluids. We employ a classical version of this relation to investigate the dynamics of polymer drag-reduced channel flows, particularly in the high-extent drag reduction (HDR) regime which is known to exhibit strong space-time intermittency. We show that high drag is not created instantaneously by near-wall coherent vortex structures as assumed in prior works. These predominantly spanwise near-wall vortex structures can produce a net "up-gradient" flux of vorticity toward the wall, which instead *reduces* instantaneous drag. Increase of wall vorticity and skin friction due to this up-gradient flux occurs after an apparent lag of several advection times, increasing with the Weissenberg number. This increasing lag appears to be due to polymer damping of up-gradient nonlinear vorticity transport that arises from large-scale eddies in the logarithmic layer. The relatively greater polymer damping of down-gradient transport due to small-scale eddies results in lower net vorticity flux and hence lower drag. The Josephson-Anderson relation thus provides an exact tool to diagnose the mechanism of polymer drag reduction in terms of vorticity dynamics and it explains also prior puzzling observations on transient drag reduction, as for centerline-release experiments in pipe flow.

DOI: 10.1103/PhysRevE.111.015105

I. INTRODUCTION

Turbulent pipe flows driven by an applied pressure head suffer frictional drag much larger than that in laminar flows, resulting in enhanced dissipation of the input energy. Remarkably, it was discovered by Toms in 1949 that the pressure drop for dilute polymer solutions (10–100 wppm) passing through a pipe is substantially lower than that for the pure solvent at the same flow rate [1]. Crucially, this *polymer drag reduction* effect occurs only for turbulent flow. In fact, the mean velocity profile of the turbulent polymeric flow becomes more similar to the laminar profile, with significantly reduced mean wall vorticity and skin friction. The phenomenon has important practical applications, such as efficient fluid transport in oil pipelines [2], firehoses [3], and irrigation systems [4]. Nevertheless, the underlying physical mechanism remains mysterious despite notable attempts [5,6] and intensive efforts up to the present time [7–10]. The solution of this long-standing puzzle could have wider implications since the maximum reduced drag by polymer additives, up to 80%, substantially exceeds that achieved by other methods, which might be improved with deeper understanding of the physics. More fundamentally, the lack of a widely accepted theory of polymer drag reduction reflects essential incompleteness in our understanding of the origin of enhanced turbulent drag and dissipation.

It has long been speculated that the polymers, because of their small size, might affect primarily the microscale turbulent vortices near the wall [11] and many studies have helped to elucidate the interactions by which polymers weaken such vortices and diminish their numbers [12–21]. However, despite great insight provided by these previous works, none have linked vorticity quantitatively with drag, resorting instead to heuristic arguments regarding the role of near-wall, quasistreamwise vortices in momentum transfer to the wall. In fact, there is an exact connection between vorticity dynamics and drag well-known in the theory of type-II superconductors and superfluids, the *Josephson-Anderson (JA) relation* [22,23]. This result relates the voltage drop in superconductors to the nucleation and motion of magnetic vortices across the background supercurrent. This relation has proved the key to the solution of the "drag reduction" problem in high-temperature superconductors. The remedy in that case is to pin the vortices by disorder, preventing their motion and reducing the voltage drop to zero [24–26].

The JA relation applies also to classical fluids [23] and especially in the "detailed relation" of Huggins [27] has been extended to a result which is local in both space and time. The relation instantaneously equates the flux of vorticity across a background potential to the work done by the total pressure of rotational flow, providing a unified explanation for drag in both external [28] and internal flows [27]. Classical vorticity differs from quantum vorticity, however, by the ability of individual lines to increase strength under stretching [see the Supplemental Material (SM) [29], which also contains Refs. [23–26,30–49], Sec. S1]. Lighthill [31] exploited this property to explain the remarkable concentration of spanwise vorticity near the wall in turbulent flows. His insight has been verified that classical vorticity dynamics near the wall is an intense competition between "down-gradient" transport out from the wall due to viscosity and turbulent advection, which smoothes wall-normal gradients of spanwise vorticity, and

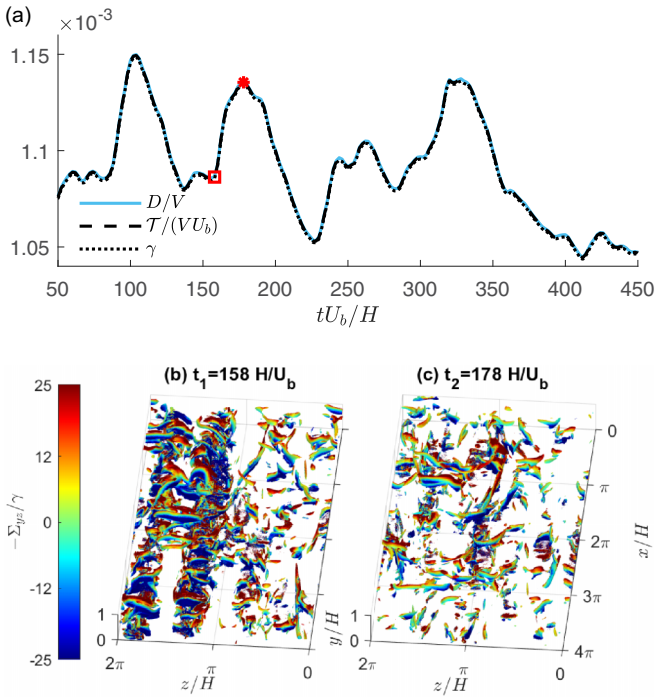

FIG. 1. Time series shown in panel (a) provide direct numerical verification of the detailed JA relation. Vortical structures identified by isosurfaces of $Q = 0.1$ are shown for instants (b) t_1 and (c) t_2, respectively marked in panel (a) by "□" and "∗". (a) Instantaneous skin friction D, volume-integrated vorticity flux $\mathcal{T}$", and pressure gradient $\gamma = \mathcal{W}/(VU_b)$", all normalized by U_b^2/H", (b) $t_1 = 158H/U_b$, and (c) $t_2 = 176H/U_b$.

"up-gradient" transport toward the wall due to vortex stretching, which sharpens gradients [44,45]. This competition has not been addressed in prior studies of polymer-vortex interactions, which have focused solely on how the vortex lifting and "bursting" are reduced [12–21]. We exploit the JA relation in a form suitable for periodic flows [50,51] to reveal the role played by vortical structures in producing both up-gradient and down-gradient fluxes, extending prior studies of Newtonian turbulent flow through pipes and channels [32,45,52]. In particular, we explain how polymer additives modify the vorticity dynamics to achieve reduced drag instantaneously, specifically in the high-extent drag reduction (HDR) regime which exhibits significant intermittency in space and time (e.g., see Fig. 1).

II. HUGGINS' DETAILED RELATION

The Navier-Stokes equations govern the flow velocity $\mathbf{u}$ of a polymer solution, with added body force $\mathbf{b} = \boldsymbol{\nabla}\cdot\boldsymbol{\sigma}_p$ due to polymer stress. The flow equations are rewritten as [32,53]

$$\partial_t u_i = (1/2)\epsilon_{ijk}\Sigma_{jk} - \partial_i h, \quad \partial_j u_j = 0, \tag{1}$$

where $h = p + |\mathbf{u}|^2/2$ is the *total pressure*, including both the hydrostatic and the dynamic pressures, and where

$$\Sigma_{ij} = u_i\omega_j - u_j\omega_i - \beta\nu(\partial_i\omega_j - \partial_j\omega_i) + \epsilon_{ijk}b_k \tag{2}$$

is the antisymmetric *vorticity flux tensor*, giving the flux of the jth vorticity component in the ith coordinate direction. The first term in Eq. (2) represents the advective transport of vorticity, the second represents transport by nonlinear stretching and tilting, the third represents viscous transport, and the fourth represents transport of vorticity perpendicular to body force $\mathbf{b}$, due to the Magnus effect [45,52]. Here, ν is the total fluid kinematic viscosity and the ratio $\beta \equiv \mu_s/(\mu_s + \mu_p)$, where μ_s and μ_p are contributions to total dynamic viscosity by the Newtonian solvent and the polymer additive at zero external shear. To derive the Huggins' relation, any model of polymer stress would suffice, but in our numerical studies in this article we adopt the finite extensible nonlinear elastic model with the Peterlin approximation (FENE-P) [54], which solves an additional equation for the conformation tensor c_{ij} describing the end-to-end deformation of polymer chains averaged over realizations of thermal noise:

$$\partial_t c_{ij} + u_k\partial_k c_{ij} = c_{kj}\partial_k u_i + c_{ik}\partial_k u_j - \tau_{ij}, \tag{3}$$

with c_{ij} normalized by the equilibrium polymer length $L_{\rm eq}$, so that $c_{ij}^{\rm eq} = \delta_{ij}$. Polymer stress $\boldsymbol{\sigma}_p = \nu(1-\beta)\boldsymbol{\tau}$ is then related to the conformation tensor via the closure:

$$\tau_{ij} = \frac{1}{Wi}\left(\frac{c_{ij}}{\psi} - \frac{\delta_{ij}}{a}\right), \ \psi = 1 - \frac{c_{kk}}{L_{\rm max}^2}, \ a = 1 - \frac{3}{L_{\rm max}^2},$$

where $Wi = \lambda U_b/H$ is the Weissenberg number based on polymer relaxation time λ and the integral timescale (H/U_b), and $L_{\rm max}$ is the maximum extensibility of the polymer in units of $L_{\rm eq}$. See the SM [29],which also contains Refs. [9,12–21,55–65], Sec. S2, for limits of this model.

The "detailed relation" of Huggins [27] (see also Ref. [52]) is derived by using as a reference field the potential flow $\mathbf{u}_\phi = \boldsymbol{\nabla}\phi$ with the same normal components as $\mathbf{u}$ at inflow and outflow. In classical fluids, $\mathbf{u}_\phi$ is the Euler flow with minimum kinetic energy for those boundary conditions, according to a theorem of Kelvin [66], and in quantum fluids it is the dissipationless ground-state superflow. Huggins [27] then considered the complementary rotational velocity field $\mathbf{u}_\omega = \mathbf{u} - \mathbf{u}_\phi$ generated by the flow vorticity and its total pressure $h_\omega = h + \partial_t\phi = p_\omega + \mathbf{u}_\phi\cdot\mathbf{u}_\omega + \frac{1}{2}|\mathbf{u}_\omega|^2$, where the Bernoulli relation $\partial_t\phi + p_\phi + \frac{1}{2}|\mathbf{u}_\phi|^2 = \partial_t\phi + h_\phi = \text{const.}$ was used. The detailed JA relation then states that $\mathcal{W}_\omega = \mathcal{T}$, where

$$\mathcal{W}_\omega = \rho\int_{S_{\rm in}} h_\omega\, dA - \rho\int_{S_{\rm out}} h_\omega\, dA \tag{4}$$

is the instantaneous work by rotational pressure drop between the inlet and the outlet surfaces, $S_{\rm in}$ and $S_{\rm out}$, and

$$\mathcal{T} = -\rho\int \mathbf{u}_\phi\cdot[\mathbf{u}\times\boldsymbol{\omega} - \beta\nu\boldsymbol{\nabla}\times\boldsymbol{\omega} - (1-\beta)\nu\boldsymbol{\nabla}\cdot\boldsymbol{\tau}]\, dV$$
$$= -\frac{1}{2}\rho\int \epsilon_{ijk}u_{\phi i}\Sigma_{jk}\, dV. \tag{5}$$

is the space-integrated flux of vorticity across the streamlines of the potential flow. Note that the work $\mathcal{W}_\phi$ done by total potential pressure h_ϕ time-averages to zero because of the Bernoulli relation, and thus only $\mathcal{W}_\omega$ constitutes "effective work." The validity of $\mathcal{W}_\omega = \mathcal{T}$ instantaneously [see Fig. 1(a) for numerical verification] is key for explaining polymer drag reduction, which has long been understood to be intermittent in space and time [9,67]. In the present study, we use a modified potential suitable for periodic channel flows such that the relations still hold [50,51].

III. NUMERICAL RESULTS

We present data from direct numerical simulation of a streamwise periodic, pressure-driven turbulent channel with polymers modeled by Eq. (3), using a well-tested code [55,56,68] that is described in more detail in the SM [29], Sec. S2. The x direction is streamwise, y is wall normal and z is spanwise, with domain size $(L_x, L_y, L_z) = (4\pi H, 2H, 2\pi H)$. The bulk velocity U_b is held constant, with $\mathrm{Re} = HU_b/\nu = 4667$, and H is the channel half-height. The FENE-P parameters are chosen as $\beta = 0.9$, $L_{\max} = 100$, and $\mathrm{Wi} = 13.5$, yielding a mean drag reduction of 69.24% compared to a Newtonian channel at the same Re. This simulation is in the HDR regime, as documented in the SM [29] (which also contains Refs. [9,16,31,67,69,70]), Sec. S3.

The JA relation must be modified due to x periodicity [50,51], and the calculation of Eq. (5) simplifies, because the background potential velocity with plane parallel walls is given simply by the plug flow $\mathbf{u}_\phi = U_b\hat{\mathbf{x}}$, yielding $\mathcal{T}(t) = -U_b\int_V \Sigma_{yz}(t)dV = VU_b\langle -\Sigma_{yz}\rangle_V(t)$, with $\langle . \rangle_V$ representing the average over the space domain with volume V and taking $\rho = 1$. Since the simulation is at a constant bulk velocity, $\partial_t\phi = 0$, so that $\mathcal{W}_\omega(t) = \gamma(t)VU_b$, where $\gamma(t) = (p|_{\text{in}} - p|_{\text{out}})/L_x$ is the instantaneous pressure gradient. The detailed JA relation is, therefore, $\mathcal{T}(t) = \gamma(t)VU_b$, simplifying to $\langle -\Sigma_{yz}\rangle_V(t) = \gamma(t)$, instantaneously equating the volume-averaged wall-normal flux of spanwise vorticity to the streamwise pressure gradient. For a constant mass flow rate, instantaneous momentum balance implies also that the pressure-gradient force is equal to the drag force $D(t)$ due to skin friction, i.e., $\gamma(t)V = D(t)$, where $D(t) = -\int_{S_{\text{wall}}} \hat{\mathbf{x}} \cdot (\beta\nu\boldsymbol{\omega} \times \mathbf{n} + \boldsymbol{\sigma}_p \cdot \mathbf{n})dS$.

These equalities are verified in Fig. 1(a), where the time series of space-mean vorticity flux, skin friction, and pressure gradient are all plotted and agree to 0.1%. For further investigation, we mark two instants of time. The first time $t_1 = 158H/U_b$ is an instant of high vortical activity as identified by a maximum of the volume average of Q^+, the positive part of the quantity $Q = \frac{1}{2}\omega^2 - S^2$ (one-half vorticity squared minus strain squared) commonly employed in vortex-visualization [71]. The second marked time $t_2 = 178H/U_b$ is the next local maximum of drag. The vortex structures for both these instants are plotted in Figs. 1(b) and 1(c) using Q^+ isosurfaces. The first reveals that vortical activity is high at $t = t_1$, with a veritable "train" of vortices in the bottom half of the channel occupying nearly half the spanwise extent ($\pi H < z < 2\pi H$). However, this instant exhibits slightly lower than average drag, and conversely vortical activity is much lower at time $t = t_2$ of the drag maximum. These plots are a counterexample to the accepted wisdom that high rotational activity should be associated with high drag [9,10,72]. It is indeed true that intense vortices are associated with higher magnitudes of vorticity flux, as shown in Figs. 1(b) and 1(c) by coloring the structures with values of $-\Sigma_{yz}$. The strong fluxes observed at $t = t_1$ in Fig. 1(b) are in both directions, but the up-gradient flux is stronger, so that instantaneous drag is reduced by the JA relation. This behavior is illustrated in Fig. 2, which plots the instantaneous streamwise averages of both Q^+ and $-\Sigma_{yz}$ at $t = t_1$. In the location of the vortex "train" in quadrant I, the up-gradient (blue) regions clearly predominate over the down-gradient (red) regions near the wall. Evaluating the sectional contributions to $\mathcal{T}$ from each of the shown quadrants reveals that the smallest drag arises from quadrant I containing the intense vortex "train," while the largest drag results from the adjacent quadrant II with little rotational activity. Here "drag" is quantified in each quadrant by the sectional contributions to both the mean vorticity flux and the skin friction at the wall. Figures 1 and 2 show that occurrence of strong vortices does *not* imply large instantaneous drag.

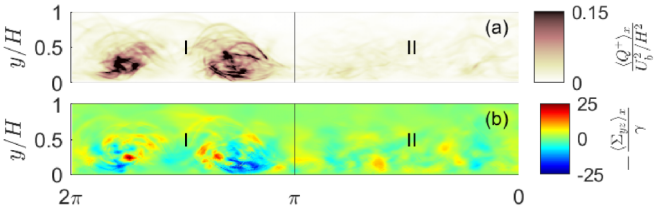

FIG. 2. At $t = t_1$, we show (a) streamwise-averaged Q^+ and (b) streamwise-averaged vorticity flux, in the bottom half of the channel. Quadrants I and II contribute 19.7% and 30.9% to net $\mathcal{T}$ or 24.2% and 27.2% to skin friction, respectively.

The nonlinear contributions for $\mathrm{Wi} = 13.5$ are pointwise the largest in the vorticity flux Σ_{yz} at $y \gtrsim 0.2H$, whereas the direct polymer contribution dominates at $y \lesssim 0.2H$; see the SM [29], Sec. S5. On the other hand, the space integral of $v\omega_z - w\omega_y = -\boldsymbol{\nabla}\cdot(\mathbf{u}u) + \partial_x(\frac{1}{2}|\mathbf{u}|^2)$ vanishes at each time instant, as a total space derivative. Thus there is no net contribution to the JA relation from the nonlinear flux in this particular flow, where 93% of the space-time average flux is contributed by the viscous term and 7% by the polymer term. Crucially, however, the nonlinear term does not have a locally vanishing average, but instead it has for every Wi, a mean which is negative (up-gradient) for $y < y_p$ and positive (down-gradient) for $y > y_p$, with $y = y_p$ being the location of the peak Reynolds stress [45,52]. Such near-wall up-gradient vorticity fluxes for Newtonian turbulence were argued in Refs. [31,44,45] to result in the increase of wall vorticity and skin friction, but this causal connection is not instantaneous. To illustrate this point, Fig. 3 plots the wall-normal profiles of the vorticity flux [$t = t_1$ panel (a), $t = t_2$ panel (b), and the spanwise vorticity fluctuation (panel (c)]. Figures 3(a) and 3(b) show that the vortex train at $t = t_1$ produces a considerable up-gradient near-wall vorticity flux, arising almost entirely from the coherent vortices in Figs. 1 and 2. In the SM [29], Sec. S4, we elaborate more on the individual contributions of nonlinear, viscous, and polymer terms. However, Figure 3(b) shows that the wall vorticity is not substantial at $t = t_1$ and only increases to very large values at $t = t_2$, when the near-wall vorticity flux also changes sign to become down-gradient. This delay between vortical activity and drag is observed in Fig. 3(c), which plots together the time series of the volume average of Q^+ and the instantaneous drag measured by $\mathcal{T}$. See also the SM [29], Sec. S9, for a movie. At least within this short time series, a correlation is observed with a time delay, with the highest correlation coefficient of 0.82 attained for a delay of $\Delta t = 13.1H/U_b$.

There is a similar delay for any Weissenberg number, increasing with Wi (see the SM [29], which also references [73], Sec. S6). The cause of this increase and for drag reduction

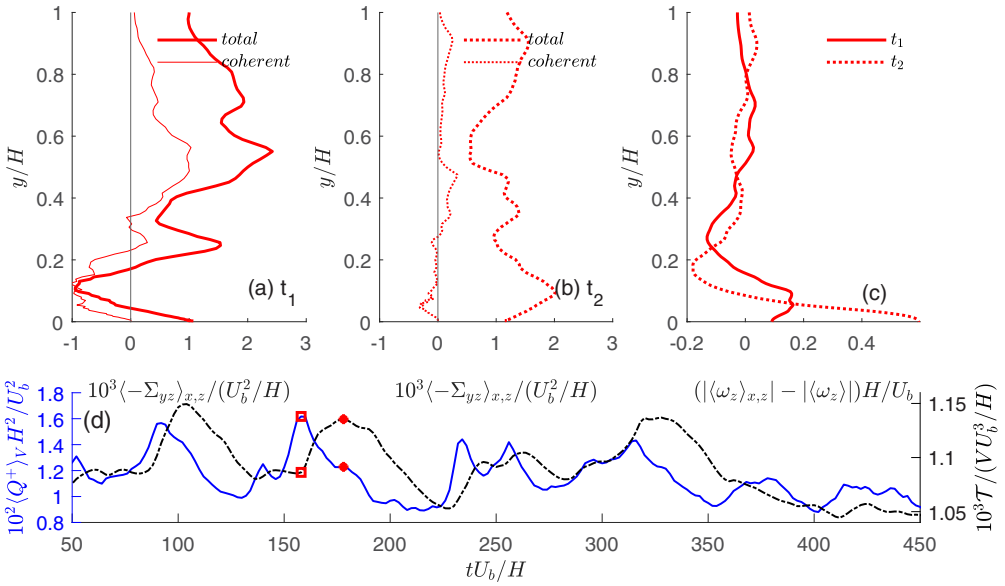

FIG. 3. Wall-normal profiles with plane-averaging $\langle\cdot\rangle_{x,z}$ of (a) instantaneous spanwise vorticity flux from the wall at $t = t_1$, both total and that from coherent vortices identified by $Q > 0.1$, (b) the same at $t = t_2$, and (c) spanwise vorticity fluctuation with $\langle\cdot\rangle \equiv \langle\cdot\rangle_{x,z,T}$ at both times $t = t_1$ and t_2. (d) Time series of $\langle Q^+\rangle_V$ and $\mathcal{T}$, with $t_1(\square)$ and $t_2(*)$ marked.

itself can be understood from a scale analysis of the mean nonlinear vorticity flux. As in Ref. [45] for Newtonian turbulence, we calculate the flux cospectrum $\phi_{v\omega_z - w\omega_y}(k_x, k_z, y)$, at a wall-normal distance y, as a function of the spanwise wave number k_z and the streamwise wave number k_x or, equivalently the premultiplied cospectrum $k_x k_z \phi_{v\omega_z - w\omega_y}$, so that integration over wavelengths $\lambda_x = 2\pi/k_x$ and $\lambda_z = 2\pi/k_z$ on a log-scale gives the net average $\langle v\omega_z - w\omega_y\rangle(y)$; see the SM [29], Sec. S7. We find that for all y in the range of the logarithmic mean profile where the flow is strongly influenced by the wall, the down-gradient transport is provided by eddies of small spanwise wavelengths $\lambda_z \lesssim 4y$ and the up-gradient transport is provided by eddies of large wavelengths $\lambda_z \gtrsim 4y$. This is illustrated by the cospectra for Wi = 0 and Wi = 13.5 plotted in Fig. 4 for $y = 0.1H < y_p$ and $y = 0.4H > y_p$. See the SM [29], Sec. S7, for other y values. The key observation is that the polymer damps nonlinear vorticity transport with increasing Wi at all y distances and all wavelengths, but the large, slow scales are less damped in the log layer than the small, rapid scales, just as would be expected by the timescale argument of Lumley [5]. For $y < y_p$, the dominant up-gradient transport thus decreases with Wi, as illustrated in Figs. 4(a) and 4(b) even as the ratio of up-gradient to down-gradient transport is increased. The near-wall, coherent vortices provide mostly up-gradient transport at Wi = 13.5 but far weaker than for Wi = 0. This weakened Lighthill mechanism [31] plausibly takes longer to concentrate spanwise vorticity at the wall and produces a weaker wall vorticity, resulting in the observed longer time delay and reduced mean skin friction.

Reduced drag is characterized also by decreased pressure drop and thus reduced mean spanwise vorticity flux across all y levels. For $y > y_p$, this outward flux in Newtonian turbulence is carried mostly by turbulent nonlinearity, but Fig. 4(c) reveals strong competition in the log layer between down-gradient transport arising from scales $\lambda_z \lesssim 4y$ and weaker up-gradient transport from scales $\lambda_z \gtrsim 4y$. As seen in Fig. 4(d) for Wi = 13.5, the polymer additive reduces both fluxes, but reduces the small-scale contribution more strongly. Thus, while mean nonlinear flux at $y > y_p$ remains down-gradient, competition becomes closer and nonlinear flux is reduced. This reduction is partially compensated by vorticity flux from the polymer force, which is also down-gradient on average for $y \gtrsim y_p$ and up-gradient for $y \lesssim y_p$ (see the SM [29], Sec. S4), reflecting the elastoinertial character of the HDR regime [70].

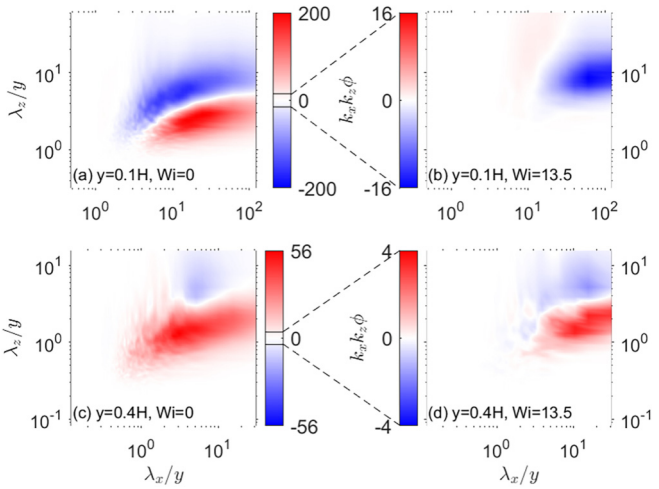

FIG. 4. Premultiplied cospectra $k_x k_z \phi_{v\omega_z - w\omega_y}(k_x, k_z)$ of mean nonlinear vorticity flux, normalized by $(-U_b^2/H)$ and magnified by 10^5. At $y = 0.1H$, net flux drops 66.7% in HDR, from -3.3×10^{-3} for panel (a), Wi = 0, to -1.1×10^{-3} for panel (b), Wi = 13.5, while the ratio of up- to down-gradient flux increases from 1.39 for panel (a) to 12.3 for panel (b). At $y = 0.4H$, net flux drops by 90.1%, from 3.37×10^{-3} for panel (c), Wi = 0 to 1.15×10^{-4} for panel (d), Wi = 13.5, while the ratio of up- to down-gradient flux increases from 0.14 for panel (c) to 0.42 for panel (d).

VI. CONCLUSIONS

We have shown how time variations of drag in the HDR regime are related to vorticity flux at each time instant via the detailed JA relation of Huggins. The number and the intensity of coherent vortices are not related to the drag magnitude instantaneously in time but instead with an apparent time delay increasing with Wi, due to reduced up-gradient vorticity transport from turbulent nonlinear dynamics. Mean drag due to net down-gradient transport is also reduced, however, because the small scales in the log layer producing nonlinear down-gradient transport are damped even more by the polymer than the large scales producing up-gradient transport. The JA relation has implications for polymer drag reduction in much more diverse settings. For example, the constancy in y of the mean wall-normal flux of spanwise vorticity ($\partial_y\langle\Sigma_{yz}\rangle = 0$) implies that the effect of the polymer is never confined to the buffer layer alone, as often claimed for the low-extent drag reduction regime [9,69], but instead mean vorticity flux must be diminished across the entire channel width. The detailed JA relation helps to explain furthermore some experiments where moderate drag reduction is observed with the injection of polymer at the centerline of a pipe, even before the polymer chains can reach the walls [74,75]. In fact, reduction of instantaneous vorticity flux anywhere in the pipe, even only over part of the volume, will reduce instantaneous drag. The detailed relation has recently been shown to be valid as well for external flows [28] and can thus elucidate polymers' effects in flow around bluff bodies such as spheres [7,76], which should show similarities to rough-walled pipes [77]. The systematic use of this relation in conjunction with more advanced numerical [78] and experimental [79] techniques will be crucial in unraveling the precise rheological mechanisms of polymer drag reduction. In fact, the detailed Josephson-Anderson relation can be applied to any other mechanism of drag reduction and provides always an exact link between vortex dynamics and drag locally both in space and in time.

ACKNOWLEDGMENTS

We thank B. Hof for valuable discussions. This work was partially supported by the Simons Foundation through Targeted Grant No. MPS-663054, "Revisiting the Turbulence Problem Using Statistical Mechanics."

[1] B. A. Toms, in *Proceedings of the First International Congress on Rheology* (1949), Vol. 2, p. 135.
[2] E. Burger, L. Chorn, and T. K. Perkins, J. Rheol. **24**, 603 (1980).
[3] R. Figueredo and E. Sabadini, Colloids Surf., A **215**, 77 (2003).
[4] M. Khalil, S. Kassab, A. Elmiligui, and F. Naoum, J. Irrig. Drain Eng. **128**, 147 (2002).
[5] J. L. Lumley, Annu. Rev. Fluid Mech. **1**, 367 (1969).
[6] P. De Gennes, Phys. A **140**, 9 (1986).
[7] C. M. White and M. G. Mungal, Annu. Rev. Fluid Mech. **40**, 235 (2008).
[8] R. Benzi and E. S. Ching, Annu. Rev. Condens. Matter Phys. **9**, 163 (2018).
[9] L. Xi, Phys. Fluids **31**, 121302 (2019).
[10] Z. Saeed and B. R. Elbing, Phys. Fluids **35**, 081304 (2023).
[11] R. W. Paterson and F. Abernathy, J. Fluid Mech. **43**, 689 (1970).
[12] E. De Angelis, C. Casciola, and R. Piva, Comput. Fluids **31**, 495 (2002).
[13] P. A. Stone and M. D. Graham, Phys. Fluids **15**, 1247 (2003).
[14] Y. Dubief, V. E. Terrapon, C. M. White, E. S. Shaqfeh, P. Moin, and S. K. Lele, Flow, Turbul. Combust. **74**, 311 (2005).
[15] A. Roy, A. Morozov, W. van Saarloos, and R. G. Larson, Phys. Rev. Lett. **97**, 234501 (2006).
[16] K. Kim, C.-F. Li, R. Sureshkumar, S. Balachandar, and R. J. Adrian, J. Fluid Mech. **584**, 281 (2007).
[17] K. Kim, R. J. Adrian, S. Balachandar, and R. Sureshkumar, Phys. Rev. Lett. **100**, 134504 (2008).
[18] A. Agarwal, L. Brandt, and T. A. Zaki, J. Fluid Mech. **760**, 278 (2014).
[19] L. Zhu, H. Schrobsdorff, T. M. Schneider, and L. Xi, J. Non-Newtonian Fluid Mech. **262**, 115 (2018).
[20] L. Zhu, X. Bai, E. Krushelnycky, and L. Xi, J. Non-Newtonian Fluid Mech. **266**, 127 (2019).
[21] L. Zhu and L. Xi, Phys. Fluids **31**, 095103 (2019).
[22] B. Josephson, Phys. Lett. **16**, 242 (1965).
[23] P. W. Anderson, Rev. Mod. Phys. **38**, 298 (1966).
[24] D. J. Bishop, P. L. Gammel, and D. A. Huse, Sci. Am. **268**, 48 (1993).
[25] W.-K. Kwok, U. Welp, A. Glatz, A. E. Koshelev, K. J. Kihlstrom, and G. W. Crabtree, Rep. Prog. Phys. **79**, 116501 (2016).
[26] A. Glatz, I. A. Sadovskyy, U. Welp, W.-K. Kwok, and G. W. Crabtree, J. Supercond. Novel Magn. **33**, 127 (2020).
[27] E. R. Huggins, Phys. Rev. A **1**, 332 (1970).
[28] G. L. Eyink, Phys. Rev. X **11**, 031054 (2021).
[29] See Supplemental Material at http://link.aps.org/supplemental/10.1103/PhysRevE.111.015105 for a comparison of classical and quantum vorticity, mathematical model and numerical methods, variations with Wi and statistical verification of an HDR regime, contributions to mean vorticity flux, profiles of instantaneous vorticity flux, correlation time of rotational activity and drag, 2D cospectra of nonlinear flux, flow fields at event pairs of high vortical activity and high drag, and animation and descriptions of timeseries.
[30] G. I. Taylor, Proc. R. Soc. London, Ser. A **135**, 685 (1932).
[31] M. J. Lighthill, in *Laminar Boundary Theory*, edited by L. Rosenhead (Oxford University, Oxford, 1963), pp. 46–113.
[32] E. R. Huggins, J. Low Temp. Phys. **96**, 317 (1994).
[33] L. Onsager, Discussion remark on C. J. Gorter, The two fluid model for helium II, Nuovo Cimento, **6** (Suppl 2), 249 (1949).
[34] R. P. Feynman, in *Progress in Low Temperature Physics*, edited by C. Gorter (North- Holland, Amsterdam, 1955), Vol. 1, pp. 17–51.
[35] A. A. Abrikosov, Dokl. Akad. Nauk SSSR **86**, 489 (1952).
[36] A. A. Abrikosov, Zh. Eksp. Teor. Fiz. **32**, 1442 (1957) [Sov. Phys. JETP **5**, 1174 (1957)].
[37] F. London, Phys. Rev. **74**, 562 (1948).
[38] E. Varoquaux, Rev. Mod. Phys. **87**, 803 (2015).
[39] Y. A. Sergeev, J. Low Temp. Phys. **212**, 251 (2023).

[40] P. Constantin and G. Iyer, Ann. Appl. Probab. **21**, 1466 (2011).
[41] G. L. Eyink, A. Gupta, and T. A. Zaki, J. Fluid Mech. **901**, A2 (2020).
[42] D. Kivotides, Phys. Rev. Lett. **96**, 175301 (2006).
[43] S. Z. Alamri, A. J. Youd, and C. F. Barenghi, Phys. Rev. Lett. **101**, 215302 (2008).
[44] M. Wang, G. L. Eyink, and T. A. Zaki, J. Fluid Mech. **941**, A32 (2022).
[45] S. Kumar, C. Meneveau, and G. Eyink, J. Fluid Mech. **974**, A27 (2023).
[46] D. Bandak, N. Goldenfeld, A. A. Mailybaev, and G. Eyink, Phys. Rev. E **105**, 065113 (2022).
[47] J. B. Bell, A. Nonaka, A. L. Garcia, and G. Eyink, J. Fluid Mech. **939**, A12 (2022).
[48] R. McMullen, J. Torczynski, and M. Gallis, Phys. Fluids **35**, 011705 (2023).
[49] G. Eyink and A. Jafari, Phys. Rev. Res. **4**, 023246 (2022).
[50] S. Kumar, Effects of walls on turbulent flow: Shear perturbations, momentum and vorticity cascades, Ph.D. thesis, Johns Hopkins University, USA, 2023.
[51] S. Kumar and G. L. Eyink, Phys. Fluids **36**, 093113 (2024).
[52] G. L. Eyink, Phys. Fluids **20**, 125101 (2008).
[53] E. R. Huggins, Phys. Rev. Lett. **26**, 1291 (1971).
[54] R. B. Bird, P. J. Dotson, and N. Johnson, J. Non-Newtonian Fluid Mech. **7**, 213 (1980).
[55] S. J. Lee and T. A. Zaki, J. Fluid Mech. **820**, 232 (2017).
[56] I. Hameduddin, C. Meneveau, T. A. Zaki, and D. F. Gayme, J. Fluid Mech. **842**, 395 (2018).
[57] M. Wang, Q. Wang, and T. A. Zaki, J. Comput. Phys. **396**, 427 (2019).
[58] T. Vaithianathan, A. Robert, J. G. Brasseur, and L. R. Collins, J. Non-Newtonian Fluid Mech. **140**, 3 (2006).
[59] R. Keunings, J. Non-Newtonian Fluid Mech. **68**, 85 (1997).
[60] Q. Zhou and R. Akhavan, J. Non-Newtonian Fluid Mech. **109**, 115 (2003).
[61] D. Vincenzi, P. Perlekar, L. Biferale, and F. Toschi, Phys. Rev. E **92**, 053004 (2015).
[62] F. Serafini, F. Battista, P. Gualtieri, and C. Casciola, Int. J. Multiphase Flow **165**, 104471 (2023).
[63] C. Clasen, J. Plog, W.-M. Kulicke, M. Owens, C. Macosko, L. Scriven, M. Verani, and G. H. McKinley, J. Rheol. **50**, 849 (2006).
[64] F. Del Giudice, S. J. Haward, and A. Q. Shen, J. Rheol. **61**, 327 (2017).
[65] S. Shaban, M. Azad, and S. Ghaemi, Phys. Fluids **30**, 125111 (2018).
[66] W. Thomson (Lord Kelvin), *Mathematical and Physical Papers* (Cambridge University Press, Cambridge, 2011).
[67] Y. Dubief, C. M. White, V. E. Terrapon, E. S. Shaqfeh, P. Moin, and S. K. Lele, J. Fluid Mech. **514**, 271 (1999).
[68] I. Hameduddin, D. F. Gayme, and T. A. Zaki, J. Fluid Mech. **858**, 377 (2019).
[69] P. S. Virk, AIChE J. **21**, 625 (1975).
[70] Y. Dubief, V. E. Terrapon, and B. Hof, Annu. Rev. Fluid Mech. **55**, 675 (2023).
[71] JCR, Hunt, A. A. Wray, and P. Moin, *Eddies, Streams, and Convergence Zones in Turbulent Flows. Center for Turbulence Research* (1988), pp. 193–208.
[72] L. Zhu and L. Xi, Phys. Rev. Fluids **6**, 014601 (2021).
[73] C. Leith, J. Appl. Meteorol. **12**, 1066 (1973).
[74] W. McComb and L. Rabie, Phys. Fluid **22**, 183 (1979).
[75] K. Kim and A. Sirviente, Flow, Turbul. Combust. **78**, 69 (2006).
[76] A. White, Nature (London) **216**, 994 (1967).
[77] P. Virk, J. Fluid Mech. **45**, 225 (1971).
[78] F. Serafini, F. Battista, P. Gualtieri, and C. M. Casciola, Phys. Rev. Lett. **129**, 104502 (2022).
[79] G. H. Choueiri, J. M. Lopez, A. Varshney, S. Sankar, and B. Hof, Proc. Natl. Acad. Sci. USA **118**, e2102350118 (2021).